

Predicting the outcome of the growth of binary solids far from equilibrium

Ranjan V. Mannige* and Stephen Whitelam†

Molecular Foundry, Lawrence Berkeley National Laboratory, 1 Cyclotron Road, Berkeley, California 94720, USA

(Received 23 July 2015; revised manuscript received 16 October 2015; published 27 April 2016)

The growth of multicomponent structures in simulations and experiments often results in kinetically trapped, nonequilibrium objects. In such cases we have no general theoretical framework for predicting the outcome of the growth process. Here we use computer simulations to study the growth of two-component structures within a simple lattice model. We show that kinetic trapping happens for many choices of growth rate and intercomponent interaction energies, and that qualitatively distinct kinds of kinetic trapping are found in different regions of parameter space. In a region in which the low-energy structure is an “antiferromagnet” or “checkerboard,” we show that the grown nonequilibrium structure displays a component-type stoichiometry that is different from the equilibrium one but is insensitive to growth rate and solution conditions. This robust nonequilibrium stoichiometry can be predicted via a mapping to the jammed random tiling of dimers studied by Flory, a finding that suggests a way of making defined nonequilibrium structures in experiment.

DOI: [10.1103/PhysRevE.93.042136](https://doi.org/10.1103/PhysRevE.93.042136)

I. INTRODUCTION

Molecular self-assembly is the spontaneous organization of components, which move around under Brownian motion but are otherwise left undisturbed, into ordered structures. Self-assembly holds considerable promise for materials science [1–4]. The goal of molecular self-assembly in the laboratory is often to make an equilibrium structure, and the laws of statistical mechanics indeed dictate that components undergoing Brownian motion will eventually build themselves into the structure of least free energy. In practical terms, however, slow dynamical processes can prevent equilibration from happening on the time scale available to the process in question [5]. In such circumstances the processes of nucleation and growth lead instead to the formation of kinetically trapped, nonequilibrium structures. Multicomponent systems, i.e., systems composed of more than one type of component, are particularly susceptible to kinetic trapping because the slow rearrangement of component types within a solid structure can prevent them from achieving their equilibrium arrangement as the solid structure grows. Frequently, the outcome of the nucleation and growth of multiple component types is an ordered crystal structure within which component types are arranged in a nonequilibrium way [6–10]. Such structures have potentially useful properties. However, predicting their component-type arrangements is not possible in general, because we cannot predict the outcome of self-assembly when that outcome is not the equilibrium structure.

Here we use simulation and analytic theory to study the component-type arrangements formed during the growth of two-component structures within a simple lattice model. In accord with several experimental results, growth results in the formation of nonequilibrium structures for a large range of growth rates and intercomponent interaction energies. In some regions of parameter space the properties of nonequilibrium structures vary continuously with growth rate, while in other regimes of parameter space these properties are insensitive to

growth rate. This qualitative behavior is similar to that seen in spinodal decomposition in the Ising antiferromagnet [11]. In a region of parameter space in which the low-energy structure is a binary “checkerboard” we show that the grown nonequilibrium structure displays a component-type stoichiometry that is insensitive both to growth rate and to the abundance of component types in solution. We show that this robust nonequilibrium stoichiometry can be predicted via a mapping to the jammed random tiling of dimers studied by Flory. These findings suggest a route to the rational design of defined nonequilibrium structures in experiment.

II. MODEL AND SIMULATION METHODS

Kinetic trapping of component types within growing multicomponent structures has a simple physical origin—the slow dynamics of particles within a solid—and so can be reproduced by simple physical models that account for this slow dynamics [6–9]. Here we consider a lattice model of growth similar to the models used in Refs. [10,12,13]. Lattice models have been widely used to study fundamental processes like nucleation and spinodal decomposition [14–17] and irreversible growth [18,19]. We focus on growth in a two-dimensional (2D) system, but we will also present results for higher dimensions. As sketched in Fig. 1(a) (also see Fig. S1 [20]), lattice sites can be unoccupied (white) or occupied by a particle of one of two types (red or blue). Red and blue particles (or components) experience color-dependent nearest-neighbor interactions (see Appendix A) of energy ϵ_{rr} , ϵ_{br} , and ϵ_{bb} , in units of $k_B T$ (which we shall set equal to unity). On a fully occupied lattice (one without white sites), and in the absence of a chemical potential difference between red and blue states these interactions are equivalent to the Ising model with magnetic field $h \equiv (\epsilon_{rr} - \epsilon_{bb})/4$ and coupling constant $J \equiv \epsilon_{br}/2 - (\epsilon_{rr} + \epsilon_{bb})/4$ [13,21]. In Fig. 1 we use J and h to indicate in an approximate fashion the regimes of phase space considered in recent simulations and experiments.

In the present paper the white, blue, and red sites also receive energetic penalties μ , $-\ln f_b^s$, and $-\ln(1 - f_b^s)$, respectively. Here μ sets the thermal weights of colored and white sites in notional “solution” (i.e., in the absence

*rvmannige@lbl.gov

†swhitelam@lbl.gov

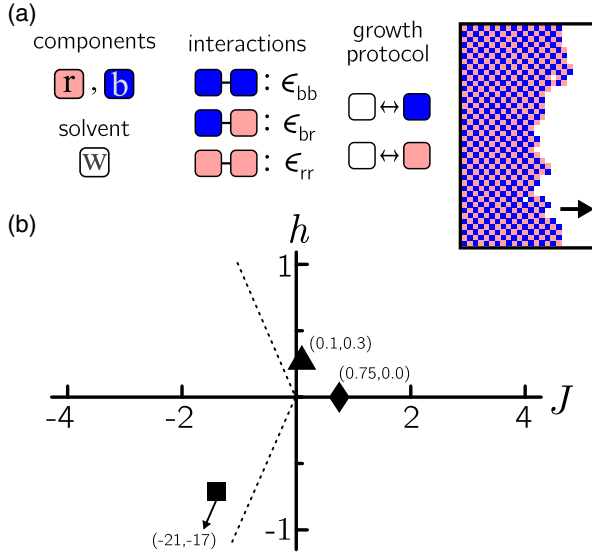


FIG. 1. (a) Schematic of the lattice model and Monte Carlo protocol we use in this paper to study growth. (b) Distinct kinds of kinetic trapping can be found for different combinations of red-blue interaction energies (see definitions of J and h in the text). In this paper we focus on the region of phase space to the left of the dotted line, where the low-energy structure is a red-blue checkerboard. We also comment on growth at points \blacksquare [13], \blacktriangle [8], and \blacklozenge [10], considered in previous studies.

of energetic interactions), and f_b^s is the notional solution fraction of colored blocks that are blue. The thermodynamic parameter μ can also be used to influence the rate of growth of a colored structure if one starts from a “white” simulation box. We evolved this model using a grand-canonical Monte Carlo procedure that respects detailed balance, and that resolves the stochastic binding and unbinding of red and blue components. Unbinding dynamics is naturally slow when components possess many colored neighbors; we also imposed a kinetic constraint that prevents any change of state of a lattice site that possesses only colored neighbors. This constraint, which preserves detailed balance, is intended to model the fact that relaxation dynamics within solid structures is slow. In what follows we shall describe growth simulations done in the presence and absence of the kinetic constraint. The latter type of simulation represents a convenient way to assess the outcome of growth on time scales longer than we could otherwise access. The dynamics of internal relaxation in the presence and absence of the kinetic constraint is different (see Appendix A)—it is much faster in the absence of the constraint—but in some regimes of parameter space the two protocols lead to similar kinetically trapped structures (Fig. S2 [20]). At infinite times, i.e., in equilibrium, the two protocols must produce the same structure, because they satisfy detailed balance with respect to the same energy function. In most simulations described below we used a 2D square lattice of 40×400 lattice sites whose long edges were periodic and whose short edges were not. We began simulations in the presence of a “seed” at the left-hand short edge of the simulation box, with the rest of the box left white, so that we could study growth without waiting for nucleation to happen.

By varying μ we could change the rate of growth of the colored assembly. In what follows we refer to “growth” simulations in which the simulation was stopped after 90% of the box become occupied by colored components, and “maturation” simulations in which structures grown in this manner were allowed to evolve for an additional 10^3 – 10^5 Monte Carlo cycles.

Note that in thermodynamic terms this lattice model is equivalent to the Blume-Emery-Griffiths model and is similar to the three-state Potts model (see, e.g., [22,23]). However, it is perhaps more useful to think of the present model as a “growing version” of the Ising model. For one, we operate in a thermodynamic regime in which white states are strongly disfavored, and so equilibrium lattices are effectively fully occupied (i.e., all sites are red or blue). The thermodynamics of the model is then to a good approximation simply that of the Ising model. For another, the behavior on which we focus is dynamic in nature, and results from the particular dynamic protocol we use, which is intended to model the growth of structures from solution. In particular, this protocol does not allow the interconversion of red and blue sites (which would correspond physically to a change of conformation of a component); if we do allow such interconversion, then relaxation to equilibrium is rapid, and the kinetically trapped states described in this paper do not arise.

III. GROWTH SIMULATIONS

Growth carried out using different choices of the inter-component energetic parameters J and h [24], shown in Fig. 1(b), is similar in the following respects (see Fig. 2). At vanishing rates of growth a structure resembling the equilibrium one is generated; at large rates of growth a “solid solution” is obtained, i.e., red and blue components are arranged randomly on the lattice in proportion to their solution proportions; and at intermediate rates of growth one obtains nonequilibrium structures that differ from both of these limiting cases. These nontrivial nonequilibrium structures can be different in different parameter regimes. For instance, using the “ferromagnetic” energy scale hierarchy shown by the symbol \blacklozenge in Fig. 1(b), nonequilibrium structures include “critical” arrangements in which red and blue component domains of a broad size distribution are present [10] (this behavior may be related to that seen in certain irreversible cellular automata [18,19]). At the parameter combination labeled \blacktriangle , nonequilibrium structures consist of large domains of the blue component within which a small red impurity fraction is found (see Fig. S3 [20]). This impurity fraction is only weakly sensitive to growth rate over some range of growth rates, a result that reproduces the qualitative outcome of growth in experiments and off-lattice simulations done by other authors [8]. The reproduction of these results by the present model suggests that it captures key physical aspects of real growth processes. Finally, at the parameter combination labeled \blacksquare in Fig. 1(b), growth results in a nonequilibrium component-type stoichiometry identical (on an **nbo** lattice) to that seen in a certain metal-organic framework; this stoichiometry is insensitive to growth rate and component solution stoichiometry over some range of those parameters [13]. As we shall show, robust nonequilibrium stoichiometry is also seen

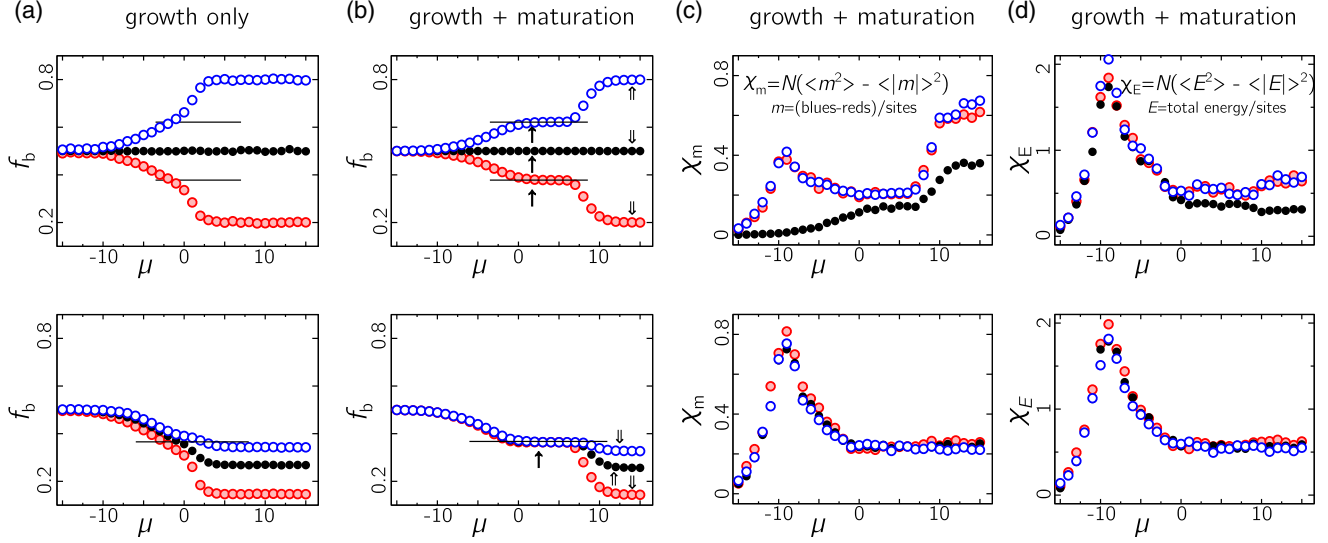


FIG. 2. The outcome of (a) growth and (b) growth-and-maturation simulations for symmetric (top panel: $\epsilon_{br} < 0 \equiv \epsilon_{rr} \equiv \epsilon_{bb}$) and asymmetric (bottom panel: $\epsilon_{br} < 0 \equiv \epsilon_{rr} \ll \epsilon_{bb}$) interaction energy hierarchies reveals the existence of “mature” nonequilibrium structures whose stoichiometry is insensitive to growth rate [(b), top panel] and growth rate and solution stoichiometry [(b), bottom panel]. Here f_b is the fraction of colored components in the grown structures that are blue, and μ is a chemical potential: the larger is μ , the more rapid is the rate of growth. Growth simulations were done using three distinct solution fractions of blue components, $f_b^s = 0.2, 0.5,$ and 0.8 [red (lightly shaded), black (solid), and blue (unfilled) circles, respectively]. Panels (c) and (d) show that near-equilibrium and far-from-equilibrium regimes are separated by a regime of large fluctuations of color and energy (measured using 10^3 independent simulations at each value of μ).

in other parameter regimes left of the dotted line in Fig. 1. Here we aim to provide a partial physical understanding of this behavior.

We start by showing in Fig. 2 the outcome of growth simulations done in the aforementioned regime of parameter space, where the red-blue energetic interaction is lower in energy than both of the like-color interactions. Here the low-energy structure, and the thermodynamically stable structure for the parameter values we shall consider, is an alternating red-blue “antiferromagnet” or checkerboard. In the top panel of Fig. 2 we show results for the parameter combination $h = 0$ (meaning that red-red and blue-blue interactions are of equal strength), while in the bottom panel we consider an asymmetric energy hierarchy for which $h \neq 0$. At low rates of growth, in both cases, the structure generated dynamically, upon 95% filling of the simulation box [panel (a)], is close in nature to the equilibrium structure, and so possesses a blue fraction (fraction of colored components that are blue) $f_b = 1/2$. For large rates of growth the structures obtained are kinetically trapped arrangements of components whose blue fraction is related to that of the notional solution (we considered three different solution stoichiometries, shown as red [lightly shaded], black [solid], and blue [unfilled] circles). At intermediate rates of growth the blue fraction of the grown structure interpolates smoothly between these limiting cases. Configuration snapshots are shown in Fig. S4 [20]. However, when allowed to further evolve or mature for 10^4 Monte Carlo sweeps [panel (b)] (in the absence of the kinetic constraint so as to effectively allow access to longer time scales), structures generated at intermediate growth rates did not evolve to equilibrium, but instead became kinetically trapped in configurations whose blue fractions display plateaus as a function of growth rate. That is, the stoichiometry of

those nonequilibrium structures is insensitive to growth rate. Furthermore, in the case of the asymmetric energetic hierarchy (bottom panel) this stoichiometry was *also* insensitive to solution stoichiometry. Near-equilibrium and far-from-equilibrium regimes are separated by a regime of large fluctuations of color and energy [panels (c) and (d)], suggesting the existence of a nonequilibrium phase transition similar to that seen in the ferromagnetic regime of parameter space [10].

Structures generated dynamically in the presence of certain energetic interactions therefore display a stoichiometry that is different from the 1:1 equilibrium one, but that is robust with respect to changes of growth rate and solution stoichiometry over a considerable range of those parameters. We call these robust nonequilibrium stoichiometries “magic numbers.” The existence of magic numbers has potential application for materials science, because it suggests that one can grow two-component solids, out of equilibrium, in a predictable manner. Magic number materials may have already been synthesized. One particular two-component metal-organic framework (MOF), called MOF-2000, displays a stoichiometry that is robust to solution stoichiometry over a considerable range [13]. The numerical value of this stoichiometry can be reproduced by the growth of magic number structures using the present model on a three-dimensional (3D) framework whose topology is appropriate to the crystal structure of MOF-2000 [13].

In physical terms, nonequilibrium structures emerge because microscopic contacts that are not the equilibrium or “native” red-blue ones (such as red-red contacts) can appear stochastically during growth and can become trapped by the arrival of additional material. In some regions of parameter space the properties of the resulting kinetically trapped structures vary continuously with growth rate and solution

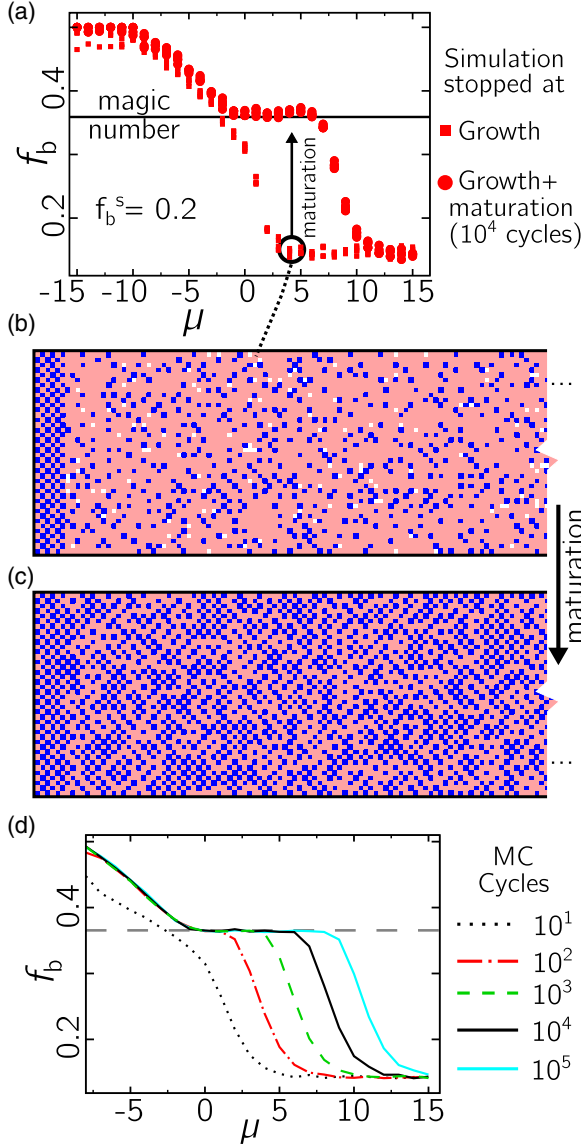


FIG. 3. Fast growth followed by maturation results in “magic number” structures. (a) The blue fraction f_b for freshly grown structures varies smoothly with growth rate between equilibrium and far-from-equilibrium limits. If allowed to evolve further, structures grown at a range of rates evolve to nonequilibrium structures that possess the same magic number stoichiometry. (b) and (c) show “grown” and “mature” structures corresponding to the points indicated in the top panel [see also Figs. S4, S5, and S6 (artificially disallowing additional nucleation at high μ also resulted in a similar magic number plateau; Fig. S7 [20])]. Maturation was stopped at 10^4 Monte Carlo cycles in (a); stopping the simulations between 10^2 and 10^3 cycles yield similar plateaus [(d); Fig. S8 [20]].

stoichiometry; in the magic number regime they do not. As shown in Fig. 3, magic number configurations, reached upon maturation of a structure after its initial growth, are long lived: evolution to the equilibrium checkerboard structure does not happen on the time scale of simulation [Fig. 3(d); Fig. S8 [20]]. Magic number structures can also be generated by zero-temperature, single-spin-flip Monte Carlo sampling of fully occupied lattices; that is, magic number structures are also

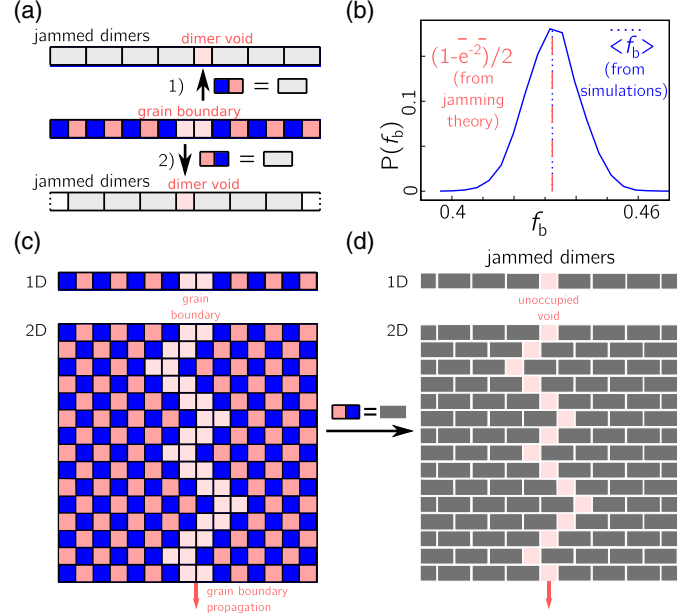


FIG. 4. (a), (b) In $d = 1$ the inherent structures of the lattice model with no white sites are, for the energetic hierarchy $\epsilon_{br} < 0 \equiv \epsilon_{rr} \ll \epsilon_{bb}$, equivalent to those produced by RSA of dimers on a lattice. (c), (d) This equivalence does not hold in higher dimensions, but there we can nonetheless use the jamming result to approximate the inherent structure result via the graphical construction shown (see text). The resulting prediction, Eq. (1), is in reasonable accord with inherent structure results for $d \leq 3$ (see Fig. 5). Because the long-time outcome of growth simulations for this energetic hierarchy are inherent structures of the lattice model with no white sites, the same magic numbers are seen in our growth simulations, i.e., in Fig. 2(b) (bottom) and Fig. 3. Thus, the nonequilibrium stoichiometry resulting from growth can be predicted via a mapping to a jammed system of dimers.

inherent structures of the lattice Hamiltonian. These inherent structures are accessible from a wide range of initial conditions (they have a large basin of attraction), and the numerical values of the associated magic numbers are dependent upon lattice connectivity and dimensionality (Fig. S9 [20]).

IV. MAPPING TO JAMMED DIMER SYSTEMS

The interaction energies used to obtain the magic numbers seen in Fig. 2 satisfy the hierarchy $\epsilon_{br} < \epsilon_{rr} \ll \epsilon_{bb}$. In words, the blue-red contact is the native or equilibrium one; red-red contacts are higher in energy but can occur during growth; and blue-blue contacts are so unfavorable that they cannot form at reasonable rates of growth. In one dimension this energetic hierarchy results in the growth of red-blue arrangements, such as those shown in Fig. 4(a), that map to a tiling of dimers with voids. “Dimers” are red-blue pairs, and “voids” are red particles. The particle-to-dimer mapping produces one of two equivalent void arrangements, as shown. The long-time outcome of our growth process then becomes equivalent to that of random sequential absorption (RSA) of dimers on a one-dimensional lattice. This problem was studied by Flory [25], who computed the dimer filling fraction to be $1 - e^{-2}$. The mean blue fraction of our equivalent red-blue structure is then

half of this value, i.e., $f_b = (1 - e^{-2})/2 \approx 0.432$. This value is indeed the mean value of the stoichiometry of inherent structures of our 1D lattice model (recall that in this regime of parameter space the matured growth configurations are also inherent structures of the model with no white sites), which we show in Fig. 4(b). Thus, the nonequilibrium stoichiometry resulting from growth can be predicted via a mapping to a jammed system of dimers.

The equivalence between our growth process and dimer deposition does not hold in dimensions greater than one. Nonetheless, we can use the Flory result to estimate numerically the magic number ratio seen in our growth simulations in 2D and 3D. Consider a periodic hypercubic lattice that possesses N lattice sites or nodes in each dimension, and so has N^d nodes in total. Each node may be occupied by one red or one blue particle. Let V be the number of void sites that exist on a connected row of N nodes in any given dimension, and assume that $V/N = e^{-2}$ [25]. Assume further that each dimension is independent, so that each void site connects to a continuous chain of void sites that extends independently into each of the remaining $d - 1$ dimensions [see Figs. 4(c) and 4(d)]. Thus, each void region contains in total VN^{d-1} voids. Therefore, summed over all independent dimensions there exist dVN^{d-1} voids in total, meaning that the void density is $dV/N = de^{-2}$. We therefore predict the nonequilibrium magic number stoichiometry of our red-blue structure, grown in d dimensions, to be

$$f_b^d = (1 - de^{-2})/2. \quad (1)$$

The magic number structures seen in the 2D growth processes whose results are reported in Fig. 2(b) (bottom) and Fig. 3 have a stoichiometry (magic number blue fraction) of 0.364 ± 0.0035 . The estimate of Eq. (1) is $f_b^2 = (1 - 2e^{-2})/2 \approx 0.365$, which agrees closely with our inherent simulation results (Fig. 5) and with the plateaus seen in our growth simulations [Fig. 3 and Fig. 2(b), bottom]. Thus the expression (1) can be used to predict, approximately, the nature of a kinetically trapped structure generated in 2D by two-component growth. In 3D the estimate (1) predicts a magic number blue fraction of $f_b^3 = 0.297$; our inherent structure simulations done in 3D display a similar magic number ratio of 0.3 ± 0.0026

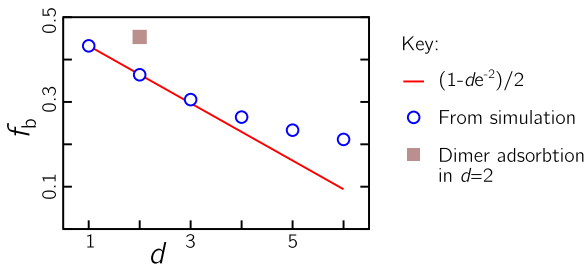


FIG. 5. Our approximate extrapolation of Flory’s dimer-packing result, Eq. (1) (red line), matches with reasonable precision the nonequilibrium magic number stoichiometries seen in inherent structures of the lattice model in $d \leq 3$ dimensions when component interactions satisfy the hierarchy $\epsilon_{br} < \epsilon_{rr} \ll \epsilon_{bb}$. The plateaus seen in growth simulations in Fig. 2(b) (bottom) and Fig. 3 have numerical values similar to the point at $d = 2$ here. For dimensions $d \geq 4$ the analytical and numerical results deviate.

(see Fig. 5). The predictions of Eq. (1) become increasingly inaccurate as the spatial dimension increases (see Fig. 5), signaling the breakdown of the approximations we used to derive the equation. But in dimensions relevant to laboratory self-assembly, for square and cubic crystal structures, we can predict approximately the stoichiometry that results from two-component kinetic trapping by analogy to a jamming problem.

We have shown that of a lattice model of two-component growth displays a rich range of phenomenology, key aspects of which reproduce behavior seen in experiments [8,13]. Growth can result in near-equilibrium structures and far-from-equilibrium structures. In certain regimes of parameter space the component-type stoichiometry of these nonequilibrium structures is independent of growth rate and solution stoichiometry, and the numerical value of this stoichiometry can be predicted via a mapping to a jammed tiling of dimers. These observations suggest that one can grow, far from equilibrium, defined two-component structures in experiment.

ACKNOWLEDGMENTS

This work was done at the Molecular Foundry at Lawrence Berkeley National Laboratory, supported by the Office of Science, Office of Basic Energy Sciences, of the U.S. Department of Energy under Contract No. DE-AC02-05CH11231.

APPENDIX: FURTHER DETAILS OF SIMULATION METHODS

Our lattice model has energy function

$$E = \sum_{i,j}^{\text{interactions}} \epsilon_{C(i)-C(j)} + \sum_i^{\text{sites}} \mu_{C(i)}. \quad (\text{A1})$$

The first sum runs over all distinct nearest-neighbor interactions, and the second sum runs over all sites. $C(i)$ in Eq. (A1) can be either w (white), b (blue), or r (red), depending on the color of node i ; $\epsilon_{C(i)-C(j)}$ is the interaction energy between colors $C(i)$ and $C(j)$; and the chemical potential $\mu_{C(i)}$ is μ , $-\ln(f_b^s)$ and $-\ln(1 - f_b^s)$ for w, b, and r, respectively. In the absence of pairwise energetic interactions (i.e., in notional “solution”), the equilibrium likelihood that a given site will be white, blue, or red is respectively $\{p_w, p_b, p_r\} = \{e^{-\mu}, f_b^s, 1 - f_b^s\}(1 + e^{-\mu})^{-1}$.

Monte Carlo simulations were done as follows. We started with a simulation box that is 400 sites wide and 40 sites high (400×40), with the first six columns populated with the equilibrium checkerboard structure (Fig. S10 [20] shows that simulations done using larger simulation boxes, e.g., those of dimensions 800×80 and 1400×140 , result in nearly identical outcomes). We selected a node at random, and proposed a change of color of that node. If the chosen node was white, we attempted to make it colored; if the chosen node was colored, we attempted to make it white. If the chosen node was white, then we proposed to make it blue with probability f_b^s ; otherwise, we proposed to make it red. No red-blue interchange was allowed, mimicking the idea that unbinding events are required in order to relax configurational degrees of freedom. To maintain detailed balance with respect to the stated energy function, the acceptance rates for these

moves were as follows (ΔE is the energy change resulting from the proposed move):

$$\begin{aligned} r \rightarrow w &: \min \{1, (1 - f_b^s) \exp[-\Delta E]\}; \\ w \rightarrow r &: \min \{1, (1 - f_b^s)^{-1} \exp[-\Delta E]\}; \\ b \rightarrow w &: \min \{1, f_b^s \exp[-\Delta E]\}; \\ w \rightarrow b &: \min \{1, (f_b^s)^{-1} \exp[-\Delta E]\}. \end{aligned}$$

The notional solution abundances of red and blue are controlled by the chemical potential term that appears in Eq. (A1) and therefore in the term ΔE . Our choice to insert blue particles with likelihood f_b^s does not by itself result in a thermodynamic bias for one color over the other (because this bias in proposal rate is countered by the nonexponential factors in the acceptance rates). Instead, we bias insertions so that the dynamics of association is consistent with the thermodynamics of the model. For instance, if blue particles are more numerous in solution than red ones, we consider it to be physically appropriate to insert blue particles into the simulation box more frequently than red particles. Consider the limit of large positive μ : the solid solution that results as the box fills irreversibly with colored particles will have a red:blue stoichiometry equal to that of the notional solution only if blue particles are inserted with likelihood f_b^s . (As a technical note, the chemical potential term present in ΔE ends up simply canceling the nonexponential factors in the acceptance rates, but we have chosen to write acceptance rates as shown in order to make clear which pieces are imposed by thermodynamics, and which pieces we have chosen for dynamical reasons). Note that temperature is not defined explicitly, but can be considered to be subsumed into the energetic parameters of the model.

We also imposed a kinetic constraint that prevents any change of state of a lattice site that possesses only colored neighbors. This constraint, motivated by work done on kinetically constrained models of glass-forming liquids [26,27], respects detailed balance. Detailed balance requires that the rates W of forward and reverse moves between microstates μ and ν satisfy

$$\rho(\mu)W(\mu \rightarrow \nu) = W(\nu \rightarrow \mu)\rho(\nu), \quad (\text{A2})$$

where $\rho(\mu)$ is the thermal weight of microstate μ . To impose a kinetic constraint for any particular forward-reverse move pair (here any move pair in which the site undergoing a change of state has as its nearest neighbors only colored sites) we scale both rates W in (A2) by $W_0 \leq 1$; in this case we take

$W_0 = 0$. This constraint does not affect the ergodicity of the system provided that one wall of the simulation box is open; otherwise, microstates corresponding to fully occupied lattices are disconnected from microstates that possess at least one unoccupied site. (One could also consider the rule that forbids a change of state from red \leftrightarrow blue to be a kinetic constraint applied to a more general spin-flip protocol.)

The kinetic constraint is intended to model the fact that relaxation dynamics within solid structures is slow. Relaxation dynamics within solid structures is then mediated by white “vacancies,” which effectively diffuse throughout the structure mediating local flips red \leftrightarrow white \leftrightarrow blue. The characteristic time for a vacancy to diffuse a distance L is $\sim L^2$, and therefore this, with L being the intervacancy separation, is the basic time scale for internal relaxation dynamics in the presence of the kinetic constraint. In some simulations we omit the kinetic constraint in order to assess the outcome of slow internal evolution on time scales longer than we could otherwise access. In this case a similar local dynamics (red \leftrightarrow white \leftrightarrow blue) occurs, but now on a basic time scale that does not scale with the distance between vacancies. In some regimes such constraint-free evolution leads rapidly to equilibrium, while in others it does not. For instance, for the intercomponent interaction energies used to obtain Fig. S3 [20], grown structures evolve quickly to equilibrium if the kinetic constraint is not used. The kinetic constraint is therefore needed in order to capture the physical character of growth seen in experiments. By contrast, for the interaction energies used to obtain Fig. 2, grown structures evolved even in the absence of the kinetic constraint fail to reach equilibrium, because of the deep kinetic traps associated with interaction energies large on the scale of $k_B T$. There we can omit the kinetic constraint in order to effectively simulate longer, and still obtain nontrivial results.

The parameter values $(\epsilon_{bb}, \epsilon_{br}, \epsilon_{rr})$ obtained from Refs. [10], [8], and [13] and marked in Fig. 1 are $(-3.5, -2, -3.5)$, $(-4.0, -3.21, -2.8)$ (also see Table S1 [20]), and $(70, -7, 0)$.

Inherent structures in $d = \{1, \dots, 6\}$ used to make Figs. 4(b) and 5 were obtained using zero-temperature single-spin-flip moves [13] (also see Fig. S9 [20]) starting from initial conditions in which all ~ 2000 sites of the periodic system are randomly colored red or blue, with equal likelihood (Fig. S9 [20]). This procedure was carried out until no more spin flips occurred. At least 100 independent inherent structures were obtained for each datapoint. As shown in Fig. S9(d) [20], the average value of the resulting f_b is insensitive to system size.

[1] George M. Whitesides and Bartosz Grzybowski, Self-assembly at all scales, *Science* **295**, 2418 (2002).
 [2] Sharon C. Glotzer and Michael J. Solomon, Anisotropy of building blocks and their assembly into complex structures, *Nat. Mater.* **6**, 557 (2007).
 [3] Daan Frenkel, Order through entropy, *Nat. Mater.* **14**, 9 (2015).
 [4] Ludovico Cademartiri and Kyle J. M. Bishop, Programmable self-assembly, *Nat. Mater.* **14**, 2 (2015).
 [5] Stephen Whitelam and Robert L. Jack, The statistical mechanics of dynamic pathways to self-assembly, *Annu. Rev. Phys. Chem.* **66**, 143 (2015).

[6] Eduardo Sanz, Chantal Valeriani, Daan Frenkel, and Marjolein Dijkstra, Evidence for Out-of-Equilibrium Crystal Nucleation in Suspensions of Oppositely Charged Colloids, *Phys. Rev. Lett.* **99**, 055501 (2007).
 [7] Baron Peters, Competing nucleation pathways in a mixture of oppositely charged colloids: Out-of-equilibrium nucleation revisited, *J. Chem. Phys.* **131**, 244103 (2009).
 [8] Anthony J. Kim, Raynaldo Scarlett, Paul L. Biancaniello, Talid Sinno, and John C. Crocker, Probing interfacial equilibration in microsphere crystals formed by DNA-directed assembly, *Nat. Mater.* **8**, 52 (2009).

- [9] Raynaldo T. Scarlett, John C. Crocker, and Talid Sinno, Computational analysis of binary segregation during colloidal crystallization with DNA-mediated interactions, *J. Chem. Phys.* **132**, 234705 (2010).
- [10] Stephen Whitelam, Lester O. Hedges, and Jeremy D. Schmit, Self-Assembly at a Nonequilibrium Critical Point, *Phys. Rev. Lett.* **112**, 155504 (2014).
- [11] Paramdeep S. Sahni, Gregory Dee, J. D. Gunton, M. Phani, Joel L. Lebowitz, and M. Kalos, Dynamics of a two-dimensional order-disorder transition, *Phys. Rev. B* **24**, 410 (1981).
- [12] Lester O. Hedges, Ranjan V. Mannige, and Stephen Whitelam, Growth of equilibrium structures built from a large number of distinct component types, *Soft Matter* **10**, 6404 (2014).
- [13] Andrew C.-H. Sue, Ranjan V. Mannige, Hexiang Deng, Dennis Cao, Cheng Wang, Felipe Gándara, Fraser Stoddart, Stephen Whitelam, and Omar M. Yaghi, Two-component metal-organic framework displaying compositional robustness to solution constitution, *Proc. Natl. Acad. Sci. USA* **112**, 5591 (2015).
- [14] K. Binder and H. Müller-Krumbhaar, Investigation of metastable states and nucleation in the kinetic Ising model, *Phys. Rev. B* **9**, 2328 (1974).
- [15] Dietrich Stauffer, Antonio Coniglio, and Dieter W. Heermann, Monte Carlo Experiment for Nucleation Rate in the Three-Dimensional Ising Model, *Phys. Rev. Lett.* **49**, 1299 (1982).
- [16] Per Arne Rikvold, H. Tomita, S. Miyashita, and Scott W. Sides, Metastable lifetimes in a kinetic Ising model: Dependence on field and system size, *Phys. Rev. E* **49**, 5080 (1994).
- [17] Lutz Maibaum, Phase Transformation Near the Classical Limit of Stability, *Phys. Rev. Lett.* **101**, 256102 (2008).
- [18] Marcel Ausloos, Nicolas Vandewalle, and Rudi Cloots, Magnetic Eden model, *Europhys. Lett.* **24**, 629 (1993).
- [19] Julián Candia and Ezequiel V. Albano, The magnetic Eden model, *Int. J. Mod. Phys. C* **19**, 1617 (2008).
- [20] See Supplemental Material at <http://link.aps.org/supplemental/10.1103/PhysRevE.93.042136> for additional figures and discussions.
- [21] Ranjan V. Mannige, Landscape of kinetically trapped binary assemblies, *J. Chem. Phys.* **143**, 214902 (2015).
- [22] Joseph B. Collins, Per Arne Rikvold, and E. T. Gawłinski, Finite-size scaling analysis of the $s = 1$ Ising model on the triangular lattice, *Phys. Rev. B* **38**, 6741 (1988).
- [23] Fa-Yueh Wu, The Potts model, *Rev. Mod. Phys.* **54**, 235 (1982).
- [24] The Ising parameters J and h defined in the main text are a convenient way to describe the three blue-red interactions ϵ_{rr} , ϵ_{br} , and ϵ_{bb} , but they provide only a partial description of the model's parameter space, which includes chemical potential terms and interactions with white sites. For instance, one can add constant terms to the ϵ parameters that leave J and h unchanged but change the energetics of the model.
- [25] Paul J. Flory, Intramolecular reaction between neighboring substituents of vinyl polymers, *J. Am. Chem. Soc.* **61**, 1518 (1939).
- [26] Juan P. Garrahan and David Chandler, Geometrical Explanation and Scaling of Dynamical Heterogeneities in Glass Forming Systems, *Phys. Rev. Lett.* **89**, 035704 (2002).
- [27] Glenn H. Fredrickson and Hans C. Andersen, Kinetic Ising Model of the Glass Transition, *Phys. Rev. Lett.* **53**, 1244 (1984).